ASTRONOMY

Accretion of a large LL parent planetesimal from a recently formed chondrule population

Graham H. Edwards* and Terrence Blackburn

Chondritic meteorites, derived from asteroidal parent bodies and composed of millimeter-sized chondrules, record the early stages of planetary assembly. Yet, the initial planetesimal size distribution and the duration of delay, if any, between chondrule formation and chondrite parent body accretion remain disputed. We use Pb-phosphate thermochronology with planetesimal-scale thermal models to constrain the minimum size of the LL ordinary chondrite parent body and its initial allotment of heat-producing ^{26}Al. Bulk phosphate $^{207}Pb/^{206}Pb$ dates of LL chondrites record a total duration of cooling $\geq$75 Ma, with an isothermal interior that cools over $\geq$30 Ma. Since the duration of conductive cooling scales with parent body size, these data require a $\geq$150-km radius parent body and a range of bulk initial $^{26}Al/^{27}Al$ consistent with the initial $^{26}Al/^{27}Al$ ratios of constituent LL chondrules. The concordance suggests that rapid accretion of a large LL parent asteroid occurred shortly after a major chondrule-forming episode.

INTRODUCTION

The ordinary chondrites (OCs) include the H, L, and LL chondrites, which derive from undifferentiated parent asteroids, or families of parent asteroids, that formed interior to Jupiter's orbit during the accretionary stages of the early Solar System (1). Dynamical and thermal models support rapid ($\lesssim$0.1 Ma) accretion time scales for these OC parent bodies within the first 3 Ma of the Solar System's first-forming solids, calcium- and aluminum-rich inclusions (CAIs) (2–6). After accretion, internal radiogenic heating coupled with conductive cooling produced a metamorphic gradient across planetesimal radii (7) that resulted in the observed range of OC petrologic types 3 to 7 (Fig. 1A). The dominant radiogenic heat source in these and other asteroidal bodies was decay of the short-lived radionuclide ^{26}Al (8). The initial solar nebula allotment of ^{26}Al relative to stable ^{27}Al, hereafter denoted $(^{26}Al/^{27}Al)_o$, is inferred from CAIs at a value of $(^{26}Al/^{27}Al)_o \sim 5 \times 10^{-5}$ (9). The homogenous evolution of $^{26}Al/^{27}Al$ in the solar nebula is supported by several lines of evidence, including chondrule Al-Mg systematics (6, 10), corroboration of ^{26}Al chronometry with the Hf-W system (11), and the modeled efficiency of nebular mixing (12). On the basis of this evidence of homogeneity, the extinct radionuclide has also served as a precise chronometer for chondrule formation. Al-Mg dates of OC chondrules indicate production at least 1 Ma after the formation of CAIs with the bulk of production at or after ~2 Ma (6), preceding the modeled time frames of OC body accretion by 10^4- to 10^5-year time scales (4, 5). Hf-W system closure in type 4 OCs at ~4 Ma after CAIs constrains the latest time of accretion (13). However, $^{207}Pb-^{206}Pb$ dates determined from sequential leaching experiments of some L group chondrules indicate protracted chondrule formation spanning 0 to 4 Ma after CAIs (14, 15), contradicting the delayed onset and short duration of chondrule formation episodes implied by Al-Mg systematics as well as the assumed homogenous nebular distribution of ^{26}Al relative to CAIs. These two chondrule production time lines predict contrasting relationships between chondrule formation and OC parent body accretion. Al-Mg systematics support a model in which chondrule formation and planetesimal accretion are closely linked temporally and, perhaps, even causally (16, 17), requiring a chondrule-forming environment that accommodates nearly contemporaneous accretion and does not need substantial chondrule transport before accretion. In contrast, chondrule $^{207}Pb-^{206}Pb$ systematics suggest that OC bodies accreted from a long-lived chondrule population that experienced protracted production and recycling events, requiring numerous chondrule-forming mechanisms active over the course of the first ~5 Ma of the Solar System and substantial chondrule transport before accretion (15).

The temporal relationship between chondrule production and accretion may be evaluated by comparing the time-dependent Al-Mg systematics of chondrules with the accretion time frame of their corresponding chondritic parent body. Most of Al-Mg studies of OC chondrules have focused on the rare LL chondrites (6), for which the most reliable ^{26}Al ages for OC chondrules come from the very primitive and minimally altered LL3.00 Semarkona. And while ^{26}Al chondrule dates provide minima for the timing of accretion, the OC accretionary time frames have been more precisely inferred from models constrained by the body-scale thermal histories recorded in OCs of various petrologic types (4, 5, 18). These longer duration (10 to 100 Ma) cooling histories of the OC parent bodies have been directly measured by temperature-sensitive radiometric systems that record the time scales of cooling, as opposed to formation, via the high-temperature diffusive loss and low-temperature retention of radiogenic daughter nuclides. These thermochronologic dates broadly exhibit an inverse correlation between petrologic type and the time scales of cooling that supports an "onion shell" model of planetesimals (13, 18–20). The onion shell model invokes gradual conductive cooling of the planetesimal over 10 to 100 Ma time scales from peak metamorphic temperatures through thermochronologic closure temperatures, resulting in cooling dates that scale with depth of residence in the planetesimal. Samples of low petrologic type cooled rapidly near the planetesimal surface and yield old cooling dates, while samples of higher petrologic type cooled slowly at depth and yield young dates (Fig. 1, A and B). Deviation from the onion shell model may occur in the case of type 7 chondrites, which are generally interpreted to reflect impact-induced heating of shallow type 5 to 6 material to the point of incipient melting (21, 22). Thus, type 7 chondrites may be expected to record early cooling consistent with shallow residence or rapid quenching after impact exhumation (Fig. 1).

Arguably, the most important thermochronologic evidence for reconstructing the parent body size and accretionary time frames from >>10-Ma cooling histories in the H and L chondrites has come
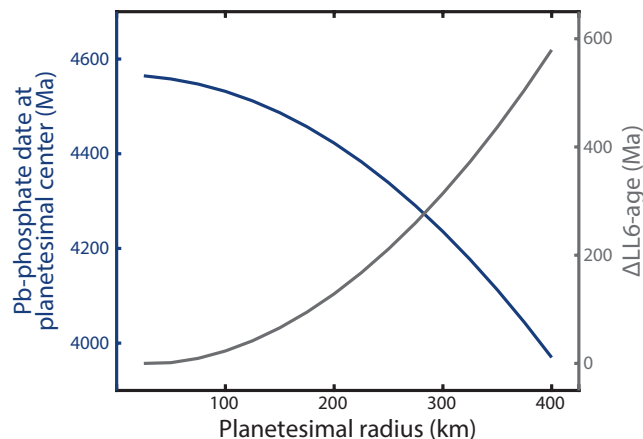
Department of Earth and Planetary Sciences, University of California Santa Cruz, Santa Cruz, CA 95064, USA.
*Corresponding author. Email: ghedwards@ucsc.edu
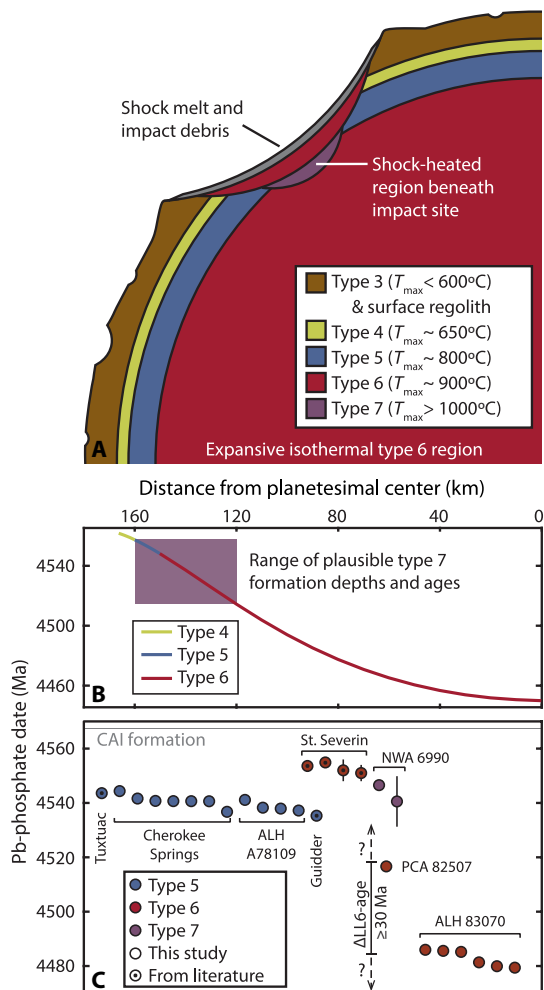
Fig. 1. Model chondrite parent body thermal structure, corresponding model Pb-phosphate cooling dates, and measured LL chondrite Pb-phosphate dates. (**A**) Schematic diagram of the distribution and peak metamorphic temperatures (T_{max}) of chondrite petrologic types in a concentrically zoned onion shell planetesimal. Type 3.0 samples are unmetamorphosed, type 6 samples experienced considerable metamorphism at silicate and FeS subsolidus conditions, and type 7 chondrites reflect heating to suprasolidus temperatures (*21, 22, 32, 51*). Depth ranges of petrologic types 4 to 6 are identified on the basis of peak metamorphic temperature ranges summarized in (*44*). We identify the depth range of type 7 formation following relationships between body size and maximum crater depths permitting planetesimal survival (*49*), assuming a 180-km radius body. (**B**) Pb-phosphate cooling dates simulated by coupled planetesimal thermal and Pb production-diffusion in phosphate models at depths corresponding to petrologic types 4 to 7 in (A). (**C**) Summary of measured LL chondrite Pb-phosphate model cooling dates from this and previous studies (*19, 23, 24*). Pb-phosphate dates are calculated using the revised bulk chondritic $^{238}U/^{235}U$ of (*14*). St. Severin and NWA 6990 reflect shallow samples affected by an early impact event and, thus, deviate from onion shell model behavior.

Fig. 2. Relationship between parent body radius and Pb-phosphate dates in a conductively cooling planetesimal. Coupled thermal and Pb production-diffusion in phosphate models predict the Pb-phosphate cooling dates at the center of the simulated planetesimal and the type 5–type 6 boundary as identified by the depth at which the average LL6 temperature (~900°C) (*51*) is reached. The Pb-phosphate date in the center of the body (blue) becomes increasingly younger for larger planetesimal radii, while increasing radius results in larger differences between this youngest LL6 age and the oldest LL6 chondrite at the LL5-LL6 boundary (ΔLL6-age, gray). This simulation assumes a 50-μm phosphate grain radius and instantaneous accretion 2.1 Ma after CAIs for $(^{26}Al/^{27}Al)_o = 5.23 \times 10^{-5}$.

from high-precision ^{207}Pb-^{206}Pb dates of bulk phosphate mineral fractions (hereafter Pb-phosphate dates). The utility of the Pb-phosphate system stems from two key characteristics: (i) Its temporal resolution can resolve protracted conductive cooling histories in excess of 100 Ma that short-lived thermochronologic systems (e.g., Al-Mg and Hf-W) cannot and (ii) its capacity to internally verify closed-system behavior with paired ^{238}U-^{206}Pb and ^{235}U-^{207}Pb systematics (see Results) that is not shared by other long-lived thermochronologic systems

(e.g., Ar-Ar and apatite/merrillite fission track). Yet, to date, the Pb-phosphate measurements of LL chondrites were limited and apparently inconsistent with onion shell cooling (*18, 19, 23, 24*). This study resolves these deficits and inconsistencies using Pb-phosphate measurements of five additional LL chondrites coupled with thermal simulations that reveal the thermal history, size, and accretionary time frame of the LL parent planetesimal.

The thermal evolution of the OC parent planetesimals has been predicted by numerical models that simulate internal radiogenic heating and conductive cooling of a spherical body (*4, 7*). Here, we compare simulated planetesimal thermal histories with measured Pb-phosphate data by using the output from model thermal histories as inputs to a model simulating Pb production and temperature-dependent diffusion in apatite (*18, 25*). The onion shell cooling scenario predicts that if a body conductively cooled unperturbed to body-wide closure of the Pb-phosphate system (the nominal closure temperature of Pb diffusion in apatite is ~500°C), the planetesimal center would record the youngest Pb-phosphate date (Fig. 1). Thus, the youngest undisturbed type 6 Pb-phosphate date measured among an OC group provides a minimum estimate of the parent body size. If any unmeasured younger type 6 samples exist and are subsequently measured, the new youngest type 6 date would imply an even larger body (Fig. 2). Further, in thermal models of large undifferentiated bodies, rapid radiogenic heating establishes an expansive isothermal interior at type 6 temperatures (*4, 7, 21*) that cools gradually over >>10 Ma (Fig. 1). Since the radius of this isothermal type 6 region will scale with planetesimal size, so too will the duration of its cooling (Fig. 2). Unlike prior studies, we neither assume the size of the simulated planetesimal (*7*) nor fix meteorite samples to particular depths of residence in the parent planetesimal to assess thermochronologic records (*4*), both of which are unknown parameters. Rather, this study interrogates the youngest measured Pb-phosphate age and the measured duration of LL6 Pb-phosphate cooling with the abovementioned

model framework to infer the minimum size of the LL parent planetesimal and the corresponding time frame of planetesimal accretion.

RESULTS

Pb-phosphate dates and the LL parent planetesimal thermal structure

Model Pb-phosphate dates from five previously unmeasured LL chondrites are reported in Fig. 1C (tables S1 and S2). The phosphate phases measured here are primarily apatite with minor amounts of merrillite (table S3). These two phases are not readily separated by standard mineral separation methods and represent variable contributions to each measured fraction. However, in the context of the present study, this variability is inconsequential since the similar ionic porosities of apatite and merrillite predict indiscernible Pb closure temperatures (18). Grain sizes of phosphate fractions ranged from 10 to 150 μm, with apparent mean effective radii of ~50 μm (fig. S1). We only report dates for phosphate fractions exhibiting ratios of radiogenic Pb (Pb*) to common Pb (Pb$_c$) >2 (table S1). Relying solely on high Pb*/Pb$_c$ measurements mitigates errors that may result from terrestrial Pb contamination and the treatment of this more radiogenic Pb$_c$ as a primitive initial Solar System composition in model age calculations (fig. S2).

We identify Cherokee Springs as an LL5 following the recommendation of (26) on the basis of prominent chondrules and a degree of recrystallization most consistent with a type 5 designation. Such an identification is further supported by its thermochronologic coincidence with other LL5 samples (Fig. 1C). The type 7 classification of Northwest Africa 6990 (NWA 6990) is supported by its granoblastic texture, absence of observable chondrules, and the coarse vein-like texture of some of its phosphates (fig. S3), analogous to those observed in the partly melted H7 Portales Valley (21, 27). The early Pb-phosphate cooling dates of NWA 6990 (LL7) and St. Severin (LL6) suggest a history of shallow residence or impact-induced exhumation to near-surface locations that resulted in early quenching (Fig. 1), consistent with the incipient-melt texture of NWA 6990 and the clastic brecciated texture of St. Severin (28). We, thus, ignore St. Severin and NWA 6990 in our assessment of an onion shell cooling history of the LL chondrite parent body. These samples reflect heating and exhumation occurring from one or more >4540 Ma impacts on the LL parent planetesimal surface that did not disrupt the entire LL parent body. Any impact powerful enough to excavate all of the other, onion shell–recording samples must have occurred no sooner than the Pb-phosphate cooling age of ALH 83070 (~4485 Ma; Fig. 1). Excluding the St. Severin breccia, the inverse correlation between LL5-LL6 petrologic types and Pb-phosphate dates indicates an onion shell structure for the LL parent body (Fig. 1C), consistent with the Hf-W systematics of LL chondrites (13).

### Evaluating Pb-phosphate dates with U-Pb systematics

The radiogenic ^{207}Pb/^{206}Pb compositions of OC phosphates permit calculation of Pb-phosphate dates with sub-million-year resolution that precisely record the 10- to 100-Ma cooling histories of OC bodies. Yet, the temperature dependence of diffusive Pb loss from phosphate minerals can leave this system susceptible to perturbation by secondary reheating events from impact-induced shock heating, as observed in the highly shocked L chondrite Sixiangkou (29). Thermal conditions associated with shock stages ≥S5 are predicted to be requisite for Pb-phosphate system partial resetting (18). The shock stages of the sub–type 7 samples studied here reflect shock stages below S4

based on visual petrographic inspection: Undulatory extinction, planar fractures, and minor opaque shock veins are present, but no pervasive melt veins were observed. Thus, we conclude Pb-phosphate system disruption is unlikely. However, any duration of open-system behavior of Pb in phosphate may be identified by evaluating the concordance between the ^{238}U-^{206}Pb and ^{235}U-^{207}Pb systems in the corresponding phosphate minerals (19, 29). Ancient reheating events may have induced the partial loss of older Pb compositions, resulting in a younger ^{207}Pb/^{206}Pb composition and corresponding Pb-phosphate date. In such instances of partial resetting, some Pb* is retained, resulting in Pb compositions that are more radiogenic than would be predicted by Pb*/U ratios alone. The resultant discordance between the ^{238}U-^{206}Pb and ^{235}U-^{207}Pb systems may be used as a sensitive monitor of Pb loss induced by open-system behavior. Pb loss and U gain drive "positive" discordance below U-Pb Concordia, while Pb gain or U loss produce "negative" discordance above U-Pb Concordia. Individual phosphate U-Pb compositions array along a mixing line between the primary cooling age and the age of the open-system event.

Pb$_c$-corrected U-Pb compositions of LL chondrite phosphate fractions are plotted in Fig. 3 with linear regressions. The model U-Pb compositions plotted in each of these Concordia plots are primarily controlled by the thermal history as described above, yet superimposed on this record are effects resulting from contemporary alteration (discussed below) as well as variation in grain size and μ (^{238}U/^{204}Pb). Given the length scale dependence of diffusion, larger phosphate crystals will record older Pb and U-Pb compositions for the same cooling histories as smaller grains. Such behavior is detrimental to linear regression of discordant fractions supposedly recording concurrent cooling ages. In addition, the Pb*/Pb$_c$ ratios of fractions of similar age scale with the μ of those fractions. Given the sensitivity of Pb* compositions to assumed Pb$_c$ for low Pb*/Pb$_c$ fractions (fig. S2), it is imperative that only grains of similar μ are regressed so that apparent patterns do not result from errors in Pb$_c$ corrections. We, thus, reject fractions that show evidence of deviation from other fractions in terms of grain size or μ (Fig. 3). In the case of ALH 83070, we have enough data to regress two separate chords showing highly similar, yet distinct, U-Pb systematics.

The OC phosphate fractions measured in this study all exhibit U-Pb discordance, particularly negative discordance (Fig. 3 and tables S1 and S2). Observations of negative discordance are common among U-Pb studies of OC phosphates (19, 30). However, in all four cases, the discordant measurements define chords that extrapolate lower intercepts nearly within 2σ of 0 Ma (Fig. 3). This is to say, the discordant arrays define mixing lines between the primary cooling ages and contemporary open-system events, which would not alter the composition of the retained Pb. Thus, the Pb* compositions of these phosphate fractions are a pristine record of the original Pb-phosphate cooling ages. Even if the nonzero intercepts reflect ancient shock heating–induced perturbations, the Pb-phosphate system is drastically less sensitive to resetting than the U-Pb system: for short-duration reheating events consistent with the minor level of offset from a nil intercept observed here, the Pb-phosphate date changes by <4% of the respective change in the ^{206}Pb/^{238}U date (fig. S4). Thus, if a nonzero intercept reflects a minor perturbation in the U-Pb system due to reheating, the effect on the Pb-phosphate system is likely negligible, confirming that the Pb-phosphate dates record the time scales of primary cooling.

The cause of the observed U-Pb discordance is U or Pb loss from phosphate weathering during terrestrial residence, a model supported
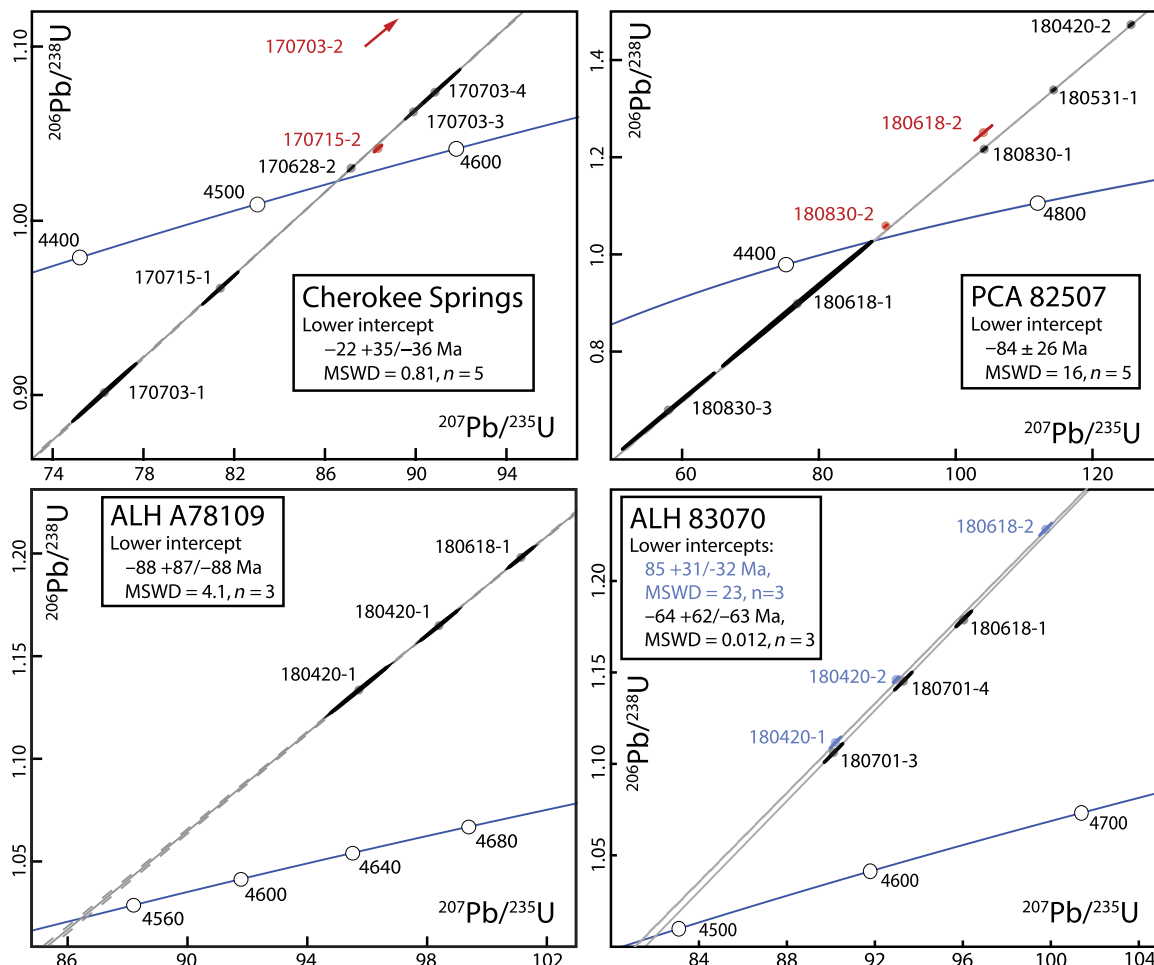
Fig. 3. Concordia diagrams of LL chondrite phosphate U-Pb compositions. Individual phosphate fractions are plotted with gray points and 2σ uncertainty ellipses traced in black. U-Pb Concordia is traced in blue with concordant ages (in Ma) identified by white circles. Fractions exhibit pervasive discordance, especially negative discordance. In all cases, U-Pb measurements plot on chords that project lower intercepts nearly within uncertainty (2σ) of a nil age. Regressions are plotted with light gray lines (uncertainty envelopes dashed). Excluded measurements (red) are rejected following criteria discussed in the text. Regressions are calculated for two groups of phosphate fractions from ALH 83070 (light blue and black). NWA 6990 is excluded because the two phosphate fractions exhibit overlapping U-Pb compositions and a chord cannot be regressed. Linear regressions are calculated (MSWD: Mean squared weighted deviation) and plotted using the algorithms of U-Pb Redux (42).

by two observations: (i) Cherokee Springs, the only studied "fall," exhibits the lowest discordance (Fig. 3), and (ii) meteorite phosphates are among the most susceptible phases to dissolution by terrestrial waters (31). Any significant U or Pb gain is precluded by the intensive cleaning procedures used in this study (see Supplementary Text). We emphasize here that although we report and interpret regressions of LL phosphate U-Pb data, the modern U and Pb loss renders the apparent U-Pb dates individually meaningless. Rather, the calculated lower intercepts simply provide a test of closed-system behavior. Because the U and Pb loss is all modern, the apparent Pb-phosphate dates accurately reflect primary cooling within the LL chondrite parent planetesimal. Only the [207]Pb-[206]Pb–derived Pb-phosphate dates have adequate temporal resolution of primary cooling and are here interpreted to discern the undisturbed onion shell thermal history of the LL planetesimal.

Interpreting the LL parent planetesimal thermal history
The LL chondrites record a ≥75-Ma Pb-phosphate cooling history and, in contrast to the relatively brief Pb-phosphate cooling time

frames of H6 and L6 chondrites (18), a >30-Ma LL6 Pb-phosphate cooling period (hereafter ΔLL6-age) defined by the difference in the Pb-phosphate dates in the LL6 chondrites PCA 82507 and ALH 83070 (Fig. 1). Since both of these chondrites record the protracted onion shell cooling of the LL planetesimal, their ΔLL6-age describes the minimum duration of Pb-phosphate cooling for the interior isothermal LL6 region (Fig. 2). The coupled models described above permit simulation of undifferentiated LL planetesimals for a range of sizes and bulk initial [26]Al/[27]Al compositions to characterize the relationship between ΔLL6-age and these two accretionary parameters (Fig. 4). Larger bodies and higher [26]Al abundances correspond to longer onion shell cooling durations and large ΔLL6-age values. In contrast, the type 6 region of bodies of both smaller size and lower [26]Al allocations cool through Pb-phosphate system closure earlier and more rapidly, thus recording relatively lower ΔLL6-age values. In Fig. 4, the contour consistent with the observed Pb-phosphate date range of the LL6 region (ΔLL6-age = 30 Ma) is traced in gray. Additional parameters are superimposed onto the parameter space in Fig. 4: the minimum planetesimal size constrained by the youngest LL6 (ALH
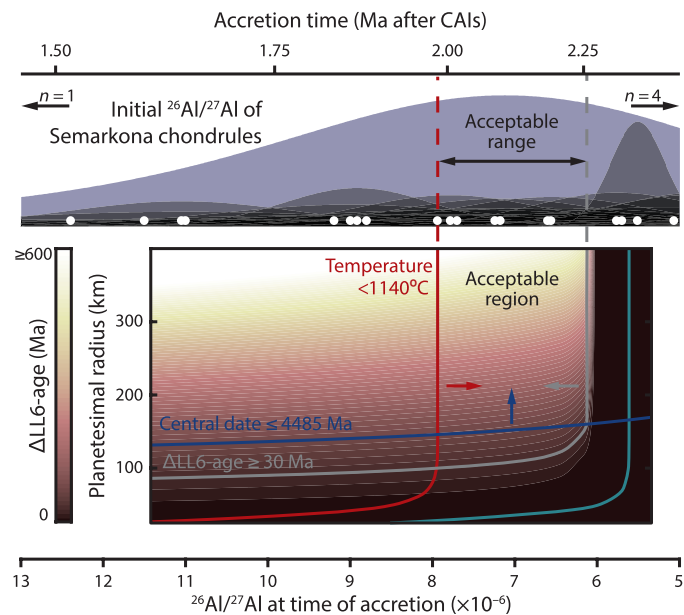
Fig. 4. Pb-phosphate thermochronologic and petrologic constraints on LL parent planetesimal size and $^{26}Al/^{27}Al$ at the time of accretion. Contours identify the date range of the modeled type 6 region (ΔLL6-age). The measured minimum ΔLL6-age of 30 Ma is traced in gray (see Supplementary Methods). The blue curve traces conditions that yield a date of 4485 Ma (ALH 83070) at the planetesimal center (labeled "Central date"), although younger dates are permissible (blue arrow, Fig. 2). The red curve traces the maximum solidus temperature (1140°C) for LL chondrite compositions (32). The teal curve traces the minimum possible metamorphic temperature (800°C) recorded by any LL6 chondrite (51). The purple kernel density estimation reflects the initial $^{26}Al/^{27}Al$ composition of Semarkona chondrules ($n = 24$) with individual chondrule $(^{26}Al/^{27}Al)_o$ means denoted by white dots and corresponding uncertainties plotted as overlying gray Gaussian bells, whereby taller bells reflect lower uncertainty measurements (10, 52–54). One chondrule $(^{26}Al/^{27}Al)$ ratio ("$n = 1$") exceeds the upper bound of the plotted $^{26}Al/^{27}Al$ range, and four ("$n = 4$") are below the lower bound. Time line is calculated from $(^{26}Al/^{27}Al)_o = 5.23 \times 10^{-5}$.

83070, ~4485 Ma) and the maximum planetesimal temperature defined by the silicate solidus (32). The absence of any achondritic or metallic meteorites that are closely affiliated with the LL chondrite group supports the assumption that bulk silicate melting did not occur in the LL parent body. Further, the early cooling date of NWA 6990 contradicts residence of at least this LL7 in the deep interior of a partially differentiated body. Collectively, the silicate solidus, youngest LL6 Pb-phosphate date, and minimum ΔLL6-age constrain both the minimum planetesimal size and the radiogenic heating budget of the LL parent body. The body must have been large enough and heated sufficiently to yield a central cooling date ≤4485 Ma, and an LL6 Pb-phosphate date range of ≥30 Ma yet remained below the silicate solidus even at its center. These requirements define a parameter space of permissible planetesimal sizes and initial ^{26}Al abundances indicated by the color-coded arrows in Fig. 4.

Minimum size of the LL parent planetesimal
Pb-phosphate and petrologic constraints require a minimum LL chondrite parent body radius of ~150 km (Fig. 4). The initial planetesimal size distribution of the nascent Solar System is a key parameter for N-body simulations of Solar System evolution and is used to both seed initial conditions and evaluate simulation outcomes (33, 34). The canonical model of the early planetesimal size distribution de-

scribes a preponderance of bodies ≤50 km in radius produced by a coagulative process of accretion (3, 35). However, the minimum LL parent body radius constrained here exceeds this canonical planetesimal size by a factor of 3. The ≥150-km LL planetesimal minimum size, combined with similar size constraints for the H and L bodies (18), supports alternative dynamical models that predict primary planetesimal populations characterized by numerous bodies reaching hundreds of kilometers in radius and formed by turbulent accretion processes (2, 34, 36). To accommodate a canonical planetesimal size (≤50-km radius) using the thermochronologic data constraints presented herein, our simulations require an unrealistic order of magnitude reduction in the modeled thermal diffusivity of the LL parent body (fig. S5).

Requisite $^{26}Al/^{27}Al$ at the time of LL parent planetesimal accretion
Large planetesimals require an internal radiogenic heat source to account for the observed metamorphism of all but the shallowest, potentially impact-heated, materials (37), and the energy available from ^{26}Al-decay stands out as the dominant heat source by orders of magnitude (8). For the minimum planetesimal size required by Pb-phosphate data, the thermal limits in Fig. 4 constrained by the silicate solidus and measured ΔLL6-age identify a range of LL parent body initial $^{26}Al/^{27}Al$ ratios spanning 6.1×10^{-6} to 7.9×10^{-6}. This $^{26}Al/^{27}Al$ range reflects bulk planetesimal $^{26}Al/^{27}Al$ compositions necessary to satisfy body-scale thermal requirements and is not sensitive to the inherent variability expected in the measurements of discrete particles (e.g., chondrules) that may have experienced complex thermal histories prior to and following accretion. Therefore, if we assume the body accreted in an environment of locally homogenized $^{26}Al/^{27}Al$ and that accretion was rapid (≲0.1 Ma) as supported by dynamical and thermal models (2–4), this range defines a 270-ka time frame in which accretion occurred (Fig. 4), independent of assumed $(^{26}Al/^{27}Al)_o$. If the process of accretion was more protracted than dynamic models predict, then a broader time window for accretion could be accommodated, although these conditions are not explored here. The measured and model data presented in Fig. 4 constrain an initial $^{26}Al/^{27}Al$ range that is insensitive to extreme variations in both body radius and thermal diffusivity for modeled planetesimals that meet the requirements of measured Pb-phosphate cooling dates (Fig. 4 and fig. S5). In summary, the initial ^{26}Al budget defined here provides an estimate for the bulk parent body $^{26}Al/^{27}Al$ ratio at the time of LL planetesimal accretion that is independent of assumptions of parent body size, thermal diffusivity, accretion time, and $(^{26}Al/^{27}Al)_o$. In contrast, the initial $^{26}Al/^{27}Al$ determined here is dependent on the assumed temperature limits of the silicate solidus and minimum LL6 peak metamorphic temperature, the assumed bulk LL chondrite Al content, and the assumed heat produced from ^{26}Al decay. Each of these parameters is well constrained (see Materials and Methods). However, changes in the modeled temperature limits expand or contract the constrained bulk planetesimal $^{26}Al/^{27}Al$ range (fig. S5), while the latter two parameters directly scale the amount of heat available for a given initial $^{26}Al/^{27}Al$. Thus, higher bulk Al and heat production values accommodate lower absolute initial $^{26}Al/^{27}Al$ ratios but do not affect the range of permissible ratios that define the window of accretion times.

DISCUSSION
Thermal limits and Pb-phosphate data define an initial $^{26}Al/^{27}Al$ composition for the bulk LL parent planetesimal that overlaps with the

initial $^{26}Al/^{27}Al$ compositions of >60% of Semarkona ferromagnesian chondrules (Fig. 4). Twenty of the 24 measured ferromagnesian Semarkona chondrules (>80%) record initial $^{26}Al/^{27}Al$ ratios that do not significantly exceed the maximum bulk planetesimal $^{26}Al/^{27}Al$ of 7.9×10^{-6} (Fig. 4). The observed agreement indicates that the bulk LL planetesimal $^{26}Al/^{27}Al$ ratio at the time of its accretion matched most of its constituent chondrules at their respective time of formation, supporting models in which chondrule production is closely followed by, and perhaps even plays a causal role in, chondrite parent body accretion (16, 17). This model is furthermore consistent with evidence from cosmogenic nuclides in chondrules that indicate rapid accretion following chondrule formation (38). These results do not rely on assumptions of $^{26}Al/^{27}Al$ homogeneity in the early nebula as has been challenged by (15). Our interpretations rely on the observation that the $^{26}Al/^{27}Al$ ratio of the LL planetesimal at the time of accretion matched the ratios of a majority of its constituent chondrules when they formed, implying concurrence of these processes under the parsimonious assumption that the chondrule-forming and accretion environments shared a $^{26}Al/^{27}Al$ reservoir. Rejecting this assumption requires the improbable alternative assumption that, despite forming in reservoirs of variable $^{26}Al/^{27}Al$, ~60 to 85% of the LL chondrules formed with initial $^{26}Al/^{27}Al$ ratios indistinguishable from that of the LL planetesimal to which they were subsequently transported and accreted.

Five of the Semarkona ferromagnesian chondrules exhibit initial $^{26}Al/^{27}Al$ compositions below the minimum initial body value of 6.1×10^{-6}, although three chondrules are within <5% of this minimum. Yet, this discordance is readily explained by evidence for postaccretion alteration of the Al-rich plagioclase and mesostasis that could have partially reset the Al-Mg system in some chondrules (39). While Semarkona reflects the least altered sample of the LL parent body, increasingly altered LL3 chondrites (type >3.00) have a greater proportion of chondrules with initial $^{26}Al/^{27}Al$ ratios lower than ~6 × 10^{-6} (e.g., 6). Alternatively, if protracted time frames of accretion and chondrule production overlapped, the shallowest LL3 material, including Semarkona, may reflect the latest materials accreted to the body after the majority of the body was assembled with a $^{26}Al/^{27}Al \geq 6.1 \times 10^{-6}$. In this case, some younger chondrules may have been incorporated along with chondrules that formed earlier. Under both scenarios, outlying low $^{26}Al/^{27}Al$ chondrules are likely not representative of the $^{26}Al/^{27}Al$ ratio during the primary phases of LL chondrule formation and planetesimal accretion. In contrast, the four measured chondrules with initial $^{26}Al/^{27}Al$ ratios significantly (2σ) in excess of 7.9×10^{-6} may reflect earlier generations incorporated into the family of newly formed chondrules that accreted onto the nascent LL parent body. However, the inherited chondrule population is a minority (~15%) of the total population, contradicting models of widespread protracted chondrule formation, storage, and recycling before planetesimal assembly (14, 15).

In summary, the broad concurrence of chondrule formation with the onset of accretion to the LL parent body supports chondrule production mechanisms that may occur several million years after CAIs and without considerable chondrule transport before accretion. Chondrule production models satisfying these requirements include planetesimal bow shocks, molten planetesimals, and high-energy collisions. The evidence we present above for the prevalence of large bodies in the nascent Solar System lends credence to bow shock models that require large planetesimals for efficient chondrule production (40). Whatever the mechanism may be, our findings imply

that chondrule-forming processes also lead to the rapid accretion of >100-km bodies from subcentimeter particles, thereby leaping the so-called "meter-size barrier" of planetary accretion (36) that dynamic models have historically failed to overcome.

MATERIALS AND METHODS

Phosphate extraction and preparation for U and Pb isotopic analysis

Samples of five LL and one L chondrite were provided by the Smithsonian and Antarctic Meteorite collections (tables S1 and S2). NWA 6990 (LL7) was purchased from M. Ouzillou of Skyfall Meteorites. Samples were selected on the basis of available sample size (>5 g of bulk material) and low grades of weathering—Cherokee Springs is a fall, and all Antarctic collection samples are weathering grade A or A/B. The Cherokee Springs, Ladder Creek, and NWA 6990 samples were crushed by hand with an agate mortar and pestle. All other samples were comminuted by electric pulse disaggregation, performed by Zirchron LLC. Crushed and fragmented samples were sieved to <500 μm, and phosphates were purified from bulk rock by magnetic and heavy liquid separations. The purified phosphate mineral separates were recovered from nonmagnetic fractions (1.4 A magnetic field, 15° slope) that sank in LST heavy liquid (2.85 g/cm^3). Given the slight acidity of LST (pH ~ 4), care was taken to promptly remove phosphate fractions from LST, minimizing exposure to <60 min. Multigrain phosphate mineral fractions were selected for isotopic analysis by optical microscopy, whereby phosphate grains were included on the basis of the absence of apparent inclusions and minimal apparent alteration or mechanical damage (fig. S1).

In an effort to minimize contributions of laboratory Pb blank and labile Pb on grain surfaces, special effort was taken to clean fractions before addition of tracer and dissolution. Selected grains were loaded into 3-ml Savillex PFA vials and rinsed two times with 18 megohm·cm deionized ultrapure water before sonication for 30 min in 500 μl of 5% ultrapure acetic acid at room temperature (Ladder Creek fractions 170608-1 and 170608-3 were sonicated for only 15 min). The acetic acid leachate was pipetted off, and leached grains were rinsed a minimum of five times with ultrapure water to dilute and remove dissolved Pb before the grains were transferred to clean 3-ml PFA vials. These "cleaned" fractions were then spiked with EARTHTIME mixed ^{202}Pb-^{205}Pb-^{233}U-^{235}U tracer (41) and dissolved in 450 to 600 μl of 6N HCl for 12 hours on a 130°C hotplate. Dissolved samples were converted to 1.1 N HBr for column introduction, and U and Pb were separated from other elements using an HBr/HCl anion exchange recipe in a 50-μl microcolumn. Pb was eluted in 6N HCl and ultrapure water, and Pb purity was improved by passing >500 μl of 1.1 N HBr over the column before eluting Pb.

To test the efficacy of the 5% acetic acid leaching procedure, fractions of ALH 83070 (180701-1 and 180701-2) were treated with an alternative cleaning method, identical to the above method with the exception that the grains were sonicated for 30 min in ultrapure water rather than 5% acetic acid. For these fractions and concurrently treated (acetic leached) fractions, the "leachates" were collected and spiked with an in-house calibrated ^{205}Pb-^{233}U-^{235}U tracer, converted to 3N HCl, and U and Pb were purified using a 50-μl microcolumn HCl-based anion-exchange chemistry. Results confirming the efficacy of the acetic acid leaching treatment are presented in the Supplementary Text.

U and Pb isotopic data were measured with isotope dilution–thermal ionization mass spectrometry (ID-TIMS) conducted on the

UCSC IsotopX X62 Thermal Ionization Mass Spectrometer. U and Pb separates were loaded onto zone-refined (99.999% purity) Re ribbon with a Si gel–0.035 M H_3PO_4 activator. Pb was measured with a peak jumping method on a Daly photomultiplier ion counting system. U was measured as an oxide by static collection on Faraday cup detectors connected to 10^{12} ohm resistance amplifier cards. Mass fractionations were calculated and corrected internally using tracer isotope pairs ^{202}Pb-^{205}Pb and ^{233}U-^{235}U. Isotopic measurements were corrected for contributions from blank, spike, and initial Pb_c (table S4), and model U-Pb and Pb-Pb dates were calculated with U-Pb Redux software (*42*). Total procedural blanks were measured throughout the duration of data acquisition and ranged from 0.3 to 1.0 pg for Pb and <0.2 pg for U. Ratios of $^{204}Pb/^{206}Pb$ and $^{207}Pb/^{206}Pb$ were calculated using calculations summarized in (*42*) to correct ID-TIMS isotopic measurements for blank and spike contributions and propagate uncertainties. We used the primordial Pb_c composition of Canyon Diablo troilite (*43*) to correct for initial Pb_c. We chose this composition over that suggested more recently by (*44*) given its long history of use in OC phosphate studies (*18*, *19*, *23*, *24*) and the fact that for measurements with Pb^*/Pb_c >2 (the threshold at which we calculate Pb-phosphate dates), the effect on the calculated age is negligible (fig. S2).

Thermal and Pb production-diffusion in phosphate models

Coupled planetesimal-scale thermal and Pb production-diffusion in phosphate codes use the model framework of (*18*), for which the same discussions of model structure, inputs, and constants therein apply here. Simulations assume instantaneous accretion of bodies following dynamical model predictions of planetesimal accretion from sub-kilometer objects on 10^4- to 10^5-year time scales for models characterized by both turbulent and coagulative accretion (*2*, *3*, *34*). We assumed an updated ^{26}Al heat production of 0.355 W/kg (*45*). We adapted physical and thermal constants to better represent LL chondrite compositions: We used an Al content of 1.18 weight % (*46*), a bulk density of $\rho = 3210$ kg/m³ (*47*), and a bulk specific heat capacity of $c_p = 950$ J kg^{-1} K^{-1}, scaled linearly on the basis of relative Fe-Ni metal abundance (*48*) from values calculated for H and L chondrites at 600 K (*49*). We used an H chondrite upper-bound thermal conductivity of $k = 4$ W m^{-1} K^{-1} after (*49*) since variation in this parameter is predominantly controlled by shock-induced porosity rather than compositional differences (*50*). Nonetheless, we explored the effects of varying thermal parameters by exploring variation in k (fig. S5). Given the relationship of thermal diffusivity (κ) to these parameters via $\kappa = k \cdot \rho^{-1} \cdot c_p^{-1}$, variations in any one variable also test the same proportional magnitude of variation in any other variable, since the κ term is ultimately used in thermal calculations.

SUPPLEMENTARY MATERIALS

REFERENCES AND NOTES

1. P. Vernazza, B. Zanda, R. P. Binzel, T. Hiroi, F. E. DeMeo, M. Birlan, R. Hewins, L. Ricci, P. Barge, M. Lockhart, Multiple and fast: The accretion of ordinary chondrite parent bodies. *Astrophys. J.* **791**, 120 (2014).
2. A. Johansen, J. S. Oishi, M.-M. Mac Low, H. Klahr, T. Henning, A. Youdin, Rapid planetesimal formation in turbulent circumstellar disks. *Nature* **448**, 1022–1025 (2007).
3. S. J. Weidenschilling, Initial sizes of planetesimals and accretion of the asteroids. *Icarus* **214**, 671–684 (2011).
4. S. Henke, H.-P. Gail, M. Trieloff, W. H. Schwarz, Thermal evolution model for the H chondrite asteroid-instantaneous formation versus protracted accretion. *Icarus* **226**, 212–228 (2013).
5. N. Sugiura, W. Fujiya, Correlated accretion ages and ε^{54}Cr of meteorite parent bodies and the evolution of the solar nebula. *Meteorit. Planet. Sci.* **49**, 772–787 (2014).
6. J. Pape, K. Mezger, A.-S. Bouvier, L. P. Baumgartner, Time and duration of chondrule formation: Constraints from ^{26}Al-^{26}Mg ages of individual chondrules. *Geochim. Cosmochim. Acta* **244**, 416–436 (2019).
7. M. Miyamoto, N. Fujii, H. Takeda, Ordinary chondrite parent body: An internal heating model. *Lunar Planet. Sci. Conf.* **12B**, 1145–1152 (1981).
8. A. Ghosh, S. J. Weidenschilling, H. Y. McSween, A. Rubin, Asteroidal heating and thermal stratification of the asteriod belt, in *Meteorites and the Early Solar System II*, D. S. Lauretta, H. Y. McSween, Eds. (University of Arizona Press, 2006), pp. 555–566.
9. B. Jacobsen, Q.-z. Yin, F. Moynier, Y. Amelin, A. N. Krot, K. Nagashima, I. D. Hutcheon, H. Palme, ^{26}Al–^{26}Mg and ^{207}Pb–^{206}Pb systematics of Allende CAIs: Canonical solar initial $^{26}Al/^{27}Al$ ratio reinstated. *Earth Planet. Sci. Lett.* **272**, 353–364 (2008).
10. J. Villeneuve, M. Chaussidon, G. Libourel, Homogeneous distribution of ^{26}Al in the Solar System from the Mg isotopic composition of chondrules. *Science* **325**, 985–988 (2009).
11. G. Budde, T. S. Kruijer, T. Kleine, Hf-W chronology of CR chondrites: Implications for the timescales of chondrule formation and the distribution of ^{26}Al in the solar nebula. *Geochim. Cosmochim. Acta* **222**, 284–304 (2018).
12. A. P. Boss, Mixing in the solar nebula: Implications for isotopic heterogeneity and large-scale transport of refractory grains. *Earth Planet. Sci. Lett.* **268**, 102–109 (2008).
13. J. L. Hellmann, T. S. Kruijer, J. A. Van Orman, K. Metzler, T. Kleine, Hf-W chronology of ordinary chondrites. *Geochim. Cosmochim. Acta* **258**, 290–309 (2019).
14. J. N. Connelly, M. Bizzarro, A. N. Krot, Å. Nordlund, D. Wielandt, M. A. Ivanova, The absolute chronology and thermal processing of solids in the solar protoplanetary disk. *Science* **338**, 651–655 (2012).
15. J. Bollard, J. N. Connelly, M. J. Whitehouse, E. A. Pringle, L. Bonal, J. K. Jørgensen, Å. Nordlund, F. Moynier, M. Bizzarro, Early formation of planetary building blocks inferred from Pb isotopic ages of chondrules. *Sci. Adv.* **3**, e1700407 (2017).
16. G. Budde, T. Kleine, T. S. Kruijer, C. Burkhardt, K. Metzler, Tungsten isotopic constraints on the age and origin of chondrules. *Proc. Natl. Acad. Sci. U.S.A.* **113**, 2886–2891 (2016).
17. C. M. O. Alexander, J. N. Grossman, D. S. Ebel, F. J. Ciesla, The formation conditions of chondrules and chondrites. *Science* **320**, 1617–1619 (2008).
18. T. Blackburn, C. M. O. Alexander, R. Carlson, L. T. Elkins-Tanton, The accretion and impact history of the ordinary chondrite parent bodies. *Geochim. Cosmochim. Acta* **200**, 201–217 (2017).
19. C. Göpel, G. Manhès, C. J. Allègre, U-Pb systematics of phosphates from equilibrated ordinary chondrites. *Earth Planet. Sci. Lett.* **121**, 153–171 (1994).
20. M. Trieloff, E. K. Jessberger, I. Herrwerth, J. Hopp, C. Fiéni, M. Ghélis, M. Bourot-Denise, P. Pellas, Structure and thermal history of the H-chondrite parent asteroid revealed by thermochronometry. *Nature* **422**, 502–506 (2003).
21. A. W. Tait, A. G. Tomkins, B. M. Godel, S. A. Wilson, P. Hasalova, Investigation of the H7 ordinary chondrite, Watson 012: Implications for recognition and classification of Type 7 meteorites. *Geochim. Cosmochim. Acta* **134**, 175–196 (2014).
22. H. Takeda, T. J. Huston, M. E. Lipschutz, On the chondrite-achondrite transition: Mineralogy and chemistry of Yamato 74160 (LL7). *Earth Planet. Sci. Lett.* **71**, 329–339 (1984).
23. A. Bouvier, J. Blichert-Toft, F. Moynier, J. D. Vervoort, F. Albarède, Pb-Pb dating constraints on the accretion and cooling history of chondrites. *Geochim. Cosmochim. Acta* **71**, 1583–1604 (2007).
24. J. H. Chen, G. J. Wasserburg, The isotopic composition of uranium and lead in Allende inclusions and meteoritic phosphates. *Earth Planet. Sci. Lett.* **52**, 1–15 (1981).
25. D. J. Cherniak, Diffusion in accessory minerals: Zircon, titanite, apatite, monazite and xenotime. *Rev. Mineral. Geochemistry.* **72**, 827–869 (2010).
26. E. Jarosewich, M. Brian, Chemical analyses with notes on one mesosiderite and seven chondrites. *Geochim. Cosmochim. Acta* **33**, 411–416 (1969).
27. A. Ruzicka, M. Killgore, D. W. Mittlefehldt, M. D. Fries, Portales Valley: Petrology of a metallic-melt meteorite breccia. *Meteorit. Planet. Sci.* **40**, 261–295 (2005).
28. A. Ruzicka, J. M. Friedrich, R. Hugo, M. Hutson, Macro- and microstructures in ordinary chondrites: Implcations for impact deformation and annealing processes, in *46th Lunar and Planetary Science Conference*, Woodlands, Texas, 16 to 20 March 2015, pp. 1544.
29. S. Li, W. Hsu, The nature of the L chondrite parent body's disruption as deduced from high-pressure phases in the Sixiangkou L6 chondrite. *Meteorit. Planet. Sci.* **53**, 2107–2122 (2018).
30. A. Blinova, Y. Amelin, C. Samson, Constraints on the cooling history of the H-chondrite parent body from phosphate and chondrule Pb-isotopic dates from Estacado. *Meteorit. Planet. Sci.* **42**, 1337–1350 (2007).
31. G. Crozaz, C. Floss, M. Wadhwa, Chemical alteration and REE mobilization in meteorites from hot and cold deserts. *Geochim. Cosmochim. Acta* **67**, 4727–4741 (2003).

32. T. E. Johnson, G. K. Benedix, P. A. Bland, Metamorphism and partial melting of ordinary chondrites: Calculated phase equilibria. *Earth Planet. Sci. Lett.* **433**, 21–30 (2016).

33. K. J. Walsh, A. Morbidelli, S. N. Raymond, D. P. O'Brien, A. M. Mandell, A low mass for Mars from Jupiter's early gas-driven migration. *Nature* **475**, 206–209 (2011).

34. J. N. Cuzzi, R. C. Hogan, W. F. Bottke, Towards initial mass functions for asteroids and Kuiper belt objects. *Icarus* **208**, 518–538 (2010).

35. J. E. Chambers, Planetary accretion in the inner Solar System. *Earth Planet. Sci. Lett.* **223**, 241–252 (2004).

36. A. Morbidelli, W. F. Bottke, D. Nesvorný, H. F. Levison, Asteroids were born big. *Icarus* **204**, 558–573 (2009).

37. J. D. Gilmour, M. J. Filtness, Dissipation of the Solar System's debris disk recorded in primitive meteorites. *Nat. Astron.* **3**, 326–331 (2019).

38. A. S. G. Roth, K. Metzler, L. P. Baumgartner, I. Leya, Cosmic-ray exposure ages of chondrules. *Meteorit. Planet. Sci.* **51**, 1256–1267 (2016).

39. J. A. Lewis, R. H. Jones, Primary feldspar in the Semarkona LL3.00 chondrite: Constraints on chondrule formation and secondary alteration. *Meteorit. Planet. Sci.* **54**, 72–89 (2019).

40. M. A. Morris, A. C. Boley, in *Chondrules*, S. S. Russell, H. C. Connolly, A. N. Krot, Eds. (Cambridge Univ. Press, 2018), pp. 375–399.

41. D. J. Condon, B. Schoene, N. M. McLean, S. A. Bowring, R. R. Parrish, Metrology and traceability of U-Pb isotope dilution geochronology (EARTHTIME Tracer Calibration Part I). *Geochim. Cosmochim. Acta* **164**, 464–480 (2015).

42. N. M. McLean, J. F. Bowring, S. A. Bowring, An algorithm for U-Pb isotope dilution data reduction and uncertainty propagation. *Geochem. Geophys. Geosyst.* **12**, Q0AA18 (2011).

43. M. Tatsumoto, R. J. Knight, C. J. Allegre, Time differences in the formation of meteorites as determined from the ratio of lead-207 to lead-206. *Science* **180**, 1279–1283 (1973).

44. J. Blichert-Toft, B. Zanda, D. S. Ebel, F. Albaràde, The Solar System primordial lead. *Earth Planet. Sci. Lett.* **300**, 152–163 (2010).

45. J. Castillo-Rogez, T. V. Johnson, M. H. Lee, N. J. Turner, D. L. Matson, J. Lunine, [26]Al decay: Heat production and a revised age for Iapetus. *Icarus* **204**, 658–662 (2009).

46. K. Lodders, B. Fegley, in *Planetary Scientist's Companion* (Oxford Univ. Press, 1998), pp. 290–331.

47. D. T. Britt, S. J. G. J. Consolmagno, Stony meteorite porosities and densities: A review of the data through 2001. *Meteorit. Planet. Sci.* **38**, 1161–1180 (2003).

48. T. L. Dunn, G. Cressey, H. Y. McSween, T. J. McCoy, Analysis of ordinary chondrites using powder X-ray diffraction: 1. Modal mineral abundances. *Meteorit. Planet. Sci.* **45**, 123–134 (2010).

49. K. Yomogida, T. Matsui, Physical properties of ordinary chondrites. *J. Geophys. Res.* **88**, 9513–9533 (1983).

50. C. P. Opeil, G. J. Consolmagno, D. J. Safarik, D. T. Britt, Stony meteorite thermal properties and their relationship with meteorite chemical and physical states. *Meteorit. Planet. Sci.* **47**, 319–329 (2012).

51. V. Slater-Reynolds, H. Y. McSween Jr., Peak metamorphic temperatures in type 6 ordinary chondrites: An evaluation of pyroxene and plagioclase geothermometry. *Meteorit. Planet. Sci.* **40**, 745–754 (2005).

52. N. T. Kita, H. Nagahara, S. Togashi, Y. Morishita, A short duration of chondrule formation in the solar nebula: Evidence from [26]Al in Semarkona ferromagnesian chondrules. *Geochim. Cosmochim. Acta* **64**, 3913–3922 (2000).

53. N. G. Rudraswami, J. N. Goswami, B. Chattopadhyay, S. K. Sengupta, A. P. Thapliyal, [26]Al records in chondrules from unequilibrated ordinary chondrites: II. Duration of chondrule formation and parent body thermal metamorphism. *Earth Planet. Sci. Lett.* **274**, 93–102 (2008).

54. I. D. Hutcheon, R. Hutchison, Evidence from the Semarkona ordinary chondrite for [26]Al heating of small planets. *Nature* **337**, 238–241 (1989).

55. G. J. MacPherson, G. R. Huss, Petrogenesis of Al-rich chondrules: Evidence from bulk compositions and phase equilibria. *Geochim. Cosmochim. Acta* **69**, 3099–3127 (2005).

56. P. Vermeesch, On the visualisation of detrital age distributions. *Chem. Geol.* **312–313**, 190–194 (2012).

57. P. Vermeesch, IsoplotR: A free and open toolbox for geochronology. *Geosci. Front.* **9**, 1479–1493 (2018).

58. C. Y. Ho, M. W. Ackerman, K. Y. Wu, S. G. Oh, T. N. Havill, Thermal conductivity of ten selected binary alloy systems. *J. Phys. Chem. Ref. Data Monogr.* **7**, 959–1178 (1978).

59. A. H. Jaffey, K. F. Flynn, L. E. Glendenin, W. C. Bentley, A. M. Essling, Precision measurement of half-lives and specific activities of [235]U and [238]U. *Phys. Rev. C* **4**, 1889–1906 (1971).

60. J. Hiess, D. J. Condon, N. McLean, S. R. Noble, [238]U/[235]U systematics in terrestrial uranium-bearing minerals. *Science* **335**, 1610–1614 (2012).

Citation: G. H. Edwards, T. Blackburn, Accretion of a large LL parent planetesimal from a recently formed chondrule population. *Sci. Adv.* **6**, eaay8641 (2020).